

Article

Sensitivity Analysis of Modal Parameters of an RC Joint Subject to Progressive Damage under Cyclic Loads

Amedeo Gregori, Lorenzo Bizzarri * , Caterina D'Agostino, Angelo Aloisio , Riccardo Cirella 
and Rocco Alaggio 

Civil Environmental and Architectural Engineering Department, Università Degli Studi dell'Aquila, Via Giovanni Gronchi n.18, 67100 L'Aquila, Italy; amedeo.gregori@univaq.it (A.G.); caterina.dagostino@graduate.univaq.it (C.D.); angelo.aloisio1@univaq.it (A.A.); rocco.alaggio@univaq.it (R.A.)

* Correspondence: lorenzo.bizzarri@graduate.univaq.it

Abstract: This paper presents the results of an experimental study that focused on the gradual modification of the modal parameters of reinforced concrete beam–column frames subjected to progressive damage under cyclic loading. As is commonly found in structures of the 1970s, the specimen was characterized by the absence of specific shear reinforcement in the nodal panel. The frame modal parameters were investigated using the ambient vibrations test (AVT) as a modal identification technique. In particular, quasi-static cyclic tests with increasing amplitudes were performed on the reinforced concrete frame specimen and the modal parameters were assessed at various stages of frame degradation. By establishing a correlation between the changes in the modal parameters and the mechanical indicators of the structural damage in the frame, this study aimed to determine whether the ambient vibration tests could offer meaningful insights for evaluating the structural health of this type of structural component. As a result of the damage that occurred in the tested RC frame, the residual experimental value of the first natural frequency of the specimen was found to reduce at 52.7% of the original reference value (undamaged stage). Similarly, the residual value of the frame stiffness was found to be as low as 43.82% of the initial one. Both these results confirmed that changes when monitoring the modal frequencies may provide quantitative indexes to describe the structural health of RC frames. In combination with static tests for a direct measure of the structural stiffness variations, the AVT technique was shown to have interesting potential in detecting the type, level, and distribution of the progressive damage in civil structures. In particular, exponential and polynomial regression curves were defined to describe the decay of the first natural frequency as the structural damage increased in various parts of the frame, and it was shown that the variation in the first natural frequency was determined more by the damage on the beam than by the damage on the joint.

Keywords: reinforced concrete; beam–column joint; structural dynamics; modal identification; cyclic load tests



Citation: Gregori, A.; Bizzarri, L.; D'Agostino, C.; Aloisio, A.; Cirella, R.; Alaggio, R. Sensitivity Analysis of Modal Parameters of an RC Joint Subject to Progressive Damage under Cyclic Loads. *Buildings* **2024**, *14*, 1345. <https://doi.org/10.3390/buildings14051345>

Academic Editor: Sufen Dong

Received: 25 March 2024

Revised: 23 April 2024

Accepted: 6 May 2024

Published: 9 May 2024



Copyright: © 2024 by the authors. Licensee MDPI, Basel, Switzerland. This article is an open access article distributed under the terms and conditions of the Creative Commons Attribution (CC BY) license (<https://creativecommons.org/licenses/by/4.0/>).

1. Introduction

In existing buildings, especially the side and corner RC beam–column joints, which are subjected to a combination of the compression, bending, shear, and torsion due to ground motions, the failure mechanism is very complicated [1].

For this reason, their performance has long been recognized as a significant factor in the behavior of RC frame structures subjected to horizontal cyclic loads. For these structures, the lack of capacity design principles leads to a low shear strength of the joint, potentially leading to a shear failure that limits the deformation capacity of adjoining beams and/or columns [2]. Many tests were carried out on the seismic performance of RC frames (like columns or beam–column joints) [3–6] and they showed that these structures were designed to resist only gravity loads, and the joints were affected by brittle-type

collapse mechanisms that can compromise the stability and start the collapse of the whole structure [7]. Based on these studies, it is important to assess the seismic vulnerability of these existing structures by nondestructive testing, such as an ambient vibration test (AVT).

Indeed, forced vibration tests to detect damage in civil structures are often impractical due to operational and cost constraints. Consequently, the ambient vibration test (AVT) often emerges as the only feasible alternative method. This approach involves the use of operational modal analysis (OMA) or output-only system identification techniques using AV data acquired before and after potential structural damage.

Astroza et al. [8] identified three primary limitations and challenges associated with OMA for damage detection. Automatic operational modal analysis becomes necessary to distinguish between spurious and genuine modes. This aspect has garnered considerable research attention, resulting in numerous proposed methods over the past two decades, like [9–16]. For instance, Rainieri and Fabbrocino [17] utilized the latest advancements in fully automated modal identification under output-only conditions to validate and implement an automated system for the vibration-based structural health monitoring of historic structures. Additionally, in [18], a novel methodology that employed the stochastic covariance-driven subspace identification (SSI-COV) method, complemented by a newly developed algorithm for the automatic analysis of stabilization diagrams, is proposed. This approach was found to be effective in identifying dynamic parameters for critical structures, such as bridges. The statistical variability of identified modal properties necessitates careful investigation.

Different factors unrelated to damage, including temperature fluctuations, measurement noise, and shifts in boundary conditions and wind speeds, can induce variations in the dynamic characteristics of civil structures [18–22]. Furthermore, the uncertainty stemming from the parameter estimation method itself must be taken into account.

The availability of data from real structures experiencing actual damage and degradation processes remains extremely limited. Most full-scale tests have been performed on in situ bridge structures slated for demolition, where artificial damage (e.g., partial saw cuts in steel girders, post-tensioning tendon cuts) was introduced during the demolition process [23–26]. However, such artificial damage fails to accurately simulate natural load-induced or aging-related damage.

For instance, the Connecticut Department of Transportation and the University of Connecticut collaborated to develop a technique for continuously monitoring highway bridges using ambient traffic as an excitation force. This study demonstrated how monitoring amplitudes at natural frequencies can serve as indicators of crack development along a highway bridge [27].

While a few studies attempted to assess the modal parameters of reinforced concrete (RC) buildings under varying states of damage [15,28,29], none, except for the work by Astroza et al. [8], continuously recorded AV data or implemented an automatic system identification approach based on data collected from a real structure subjected to damage induced by realistic dynamic excitation sources.

The AVT technique is currently used in the evaluation of even complex existing structures, sometimes with serious difficulties in the interpretation of the results, especially about the actual location and level of the structural damage (if any is present) or about the level of the structural degradation. The present study's main objective was to demonstrate the suitability of monitoring the modification of the modal parameters of an RC frame to provide both quantitative and qualitative descriptions of the structural damage caused by intense cyclic loads. To address this issue, an AVT technique was carried out in parallel with the destructive test of a simple geometry RC frame. This frame was thought to represent a sample of typical old existing RC structures, usually characterized as having no stirrups in the joint; then, reinforcement was introduced to provide an improved global capacity to the structure somehow. The effectiveness of the structural reinforcement applied to the tested beam–column joint is not discussed in this paper; instead, it is to be presented in a different research paper in the near future.

The value of the AVT technique, like others, is perhaps clearest in thinking that public measures are accelerating investments in the existing building stock to enhance the seismic safety in high-risk seismic zones, although continuous monitoring to assess intervention effectiveness over time has not been consistently required. Concurrently, energy efficiency measures are also often performed on the building envelope, making subsequent structural inspections even more challenging in the post-earthquake assessment of the buildings, as well as after an extreme event. As a result, there is a growing need for rapid, continuous, and noninvasive monitoring techniques [30–32] capable of detecting changes in the structural dynamic response, especially for swiftly evaluating the structural integrity after extreme loads.

In the case of seismic events, poorly engineered beam–column joints are, among all, the most vulnerable elements in RC buildings. These joints exhibit changes in stiffness as damage progresses. Accurately estimating the evolution of joint stiffness is crucial for modeling the nonlinear dynamic response of reinforced concrete buildings. However, most experiments on beam–column joints focused on characterizing the moment–rotation curves. These relationships are challenging to measure directly from accelerometric data during an earthquake. In this study, the authors simulated the progressive damage of an RC beam–column joint, conducting discrete steps of loading and stopping the loading protocol to measure the ambient vibration response of the reinforced concrete joint. This approach aimed to estimate the modal parameters and, given the experimental moment–rotation curves, to relate the modal parameter estimates with the mechanical parameters' evolution. The novelty of this study lay in its objectives and methods. There is a lack of research in the literature linking the evolution of modal parameters of an RC joint with its mechanical response. Additionally, the authors conducted hybrid loading tests and ambient vibration measurements on the joint and designed a loading protocol with approximately 20-minute interruptions for the experimental characterization of the modal parameters.

2. Experimental Setup

The specimen examined in this study was a T-shaped reinforced concrete (RC) joint as an example of a cellular unit of an RC frame, as found in real buildings from the 1970s [33].

Positioned on a horizontal plane, the specimen was inserted on a steel loading frame securely fixed to the floor, as shown in Figure 1 and in Figure 2. As shown in Figure 1, the left end “A” was secured by a roller constraint, while the lower end “B” was supported by a hinge constraint. Please note that the tested specimen represented only a part of an ideal real frame.

In particular, the ends “A”, “B”, and “C” of the specimen corresponded to the half-length of the beam and the column of a complete frame, where the inflection points with $M = 0$ were usually located when seismic loads were considered. For this reason, the hypothesis of a fixed support was not applied and a hinge support was considered.

The picture in Figure 2 presents the actual tested specimen, offering a partial view of the experimental setup.

Figure 1 also illustrates the geometric dimensions and reinforcement details of the specimen. Both the beam and the column were characterized by a cross-sectional area of $300 \times 500 \text{ mm}^2$, with the column's overall height measuring 3200 mm and the beam's total length spanning 2500 mm. Additionally, a transverse beam with a cross-sectional area of $300 \times 500 \text{ mm}^2$ and extending 600 mm from the column face was included. This transverse beam was introduced to more accurately replicate the geometry of reinforced concrete frames found at the corner of common existing buildings to consider the influence of a beam orthogonal to the frame.

The column's reinforcement consisted of $4\phi 24$ mm steel ribbed bars set longitudinally along both of the shorter sides of the section. With reference to the beam, $2\phi 24$ mm plus $3\phi 20$ mm ribbed bars were adopted as longitudinal reinforcement (on both of the short sides of the section). The reinforcement of the short beam orthogonal to the frame consisted of a single $\phi 16$ mm longitudinal reinforced ribbed bar at each of the four corners. Transverse

reinforcement for the column and the beam included 10 mm diameter stirrups placed at intervals of 100 mm. The stirrups were deliberately excluded from the joint space to reduce its strength, and thus, induce shear failure in the joint before attaining the yield in both the beam and column branch during the simulated seismic loads.

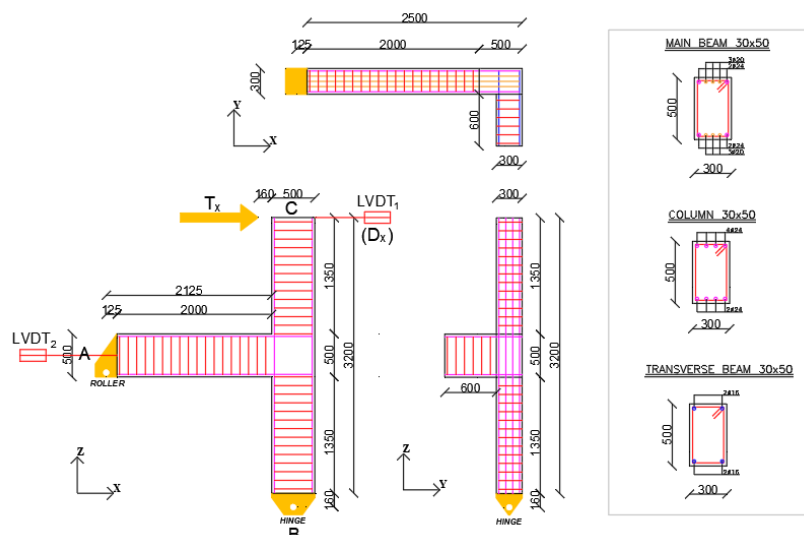


Figure 1. Various views of the specimen with details about the geometry and reinforcement.



Figure 2. Testing assembly.

Two linear variable displacement transducers (LVDTs) were used to measure the main displacement of the frame under loads. They were placed with one at the top end “C” of the column (Figure 1) and one aligned with the main beam axis at the left end “A” of the beam (Figure 1). To operate the cyclic loading in the displacement-controlled procedure, an electrically driven actuator measuring 500 kN in capacity was applied at end “C” of the column; meanwhile, a 500 kN capacity load cell was used to record the force resisted by the structure.

About the material used for the specimen preparation, the concrete was characterized by an average compressive strength of 29.3 MPa, and the reinforcing steel bars were characterized by a yield strength of 450 MPa. Please note that in Italy, only steel grade 450 is allowed for the design and construction of RC structures (B450C steel type) (NTC018). Grade 420 MPa has never been considered in the past, when the values of f_y usually

adopted were between 220 MPa and 440 MPa. Currently, only grade B450C is available on the market.

Other mechanical properties of the used materials are reported in the subsequent Table 1 with the following symbols:

- E_{cm}, E_s : Young's moduli of concrete and steel rebar, respectively;
- f_c, f_{ctm} : compression strength of concrete and tensile strength of concrete;
- f_y, f_u : yielding strength of steel rebar and ultimate strength of steel rebar;
- G_r^1 : tensile energy fracture;
- h : height of the RC specimen (from the bottom to the head column);
- γ_c, γ_s : densities of concrete and steel rebar, respectively;
- $\varepsilon_{sy}, \varepsilon_{su}$: deformations in relation to the yielding strength and ultimate strength of the steel rebar, respectively;
- ν_c, ν_s : Poisson's coefficients of concrete and steel rebar, respectively.

Table 1. Mechanical properties of the concrete (* assumed from CEB-FIB for the numerical simulations) and of the steel rebars.

Concrete						
f_c (Mpa)	f_{ctm} (Mpa)	E_{cm} (Mpa)	γ_c (N/mm ³)	ν_c (-)	G_r^1 (Nm/m ²)	
29.3	2.85	30,373	2.5×10^{-3}	0.2	0.05	
Steel						
f_y (MPa)	f_u (MPa)	E_s (MPa)	γ_s (N/mm ³)	ν_s (-)	ε_{sy} %	ε_{su} %
450	540	210,000	7.85×10^{-3}	0.29	2.14	75

More details about the experimental setup are provided in Figure 3. In particular, a total of six force balance accelerometers are shown. Their strategic placement was decided to capture the dynamic behavior of the specimen through the ambient vibration test (AVT), with the aim to achieve a thorough evaluation of the damage progression within the specimen.



Figure 3. Experimental layout with a view of the measuring devices.

In particular, the digital array accelerometric measurement chain comprised SL06 converters and FB SA10 accelerometers produced by Sara Electronic Instruments (Italy). The accelerometer had a dynamic range higher than 165 dB from 0.1 Hz to 200 Hz, with a 1 g full scale. On the other hand, the dynamic range of the digital converter was 144 dB such that the sensitivity was limited by the converter, not by the noise of the accelerometer,

which was lower. Accordingly, the sensitivity of the sensor was $0.119 \mu\text{g}/\text{count}$. The accelerometers were arranged into two measurement chains, each driven by a master recording unit connected to a Wi-Fi access point and synchronized by GPS receivers.

3. Experimental Test

To comprehensively analyze the mechanical behavior and the modal parameter changes of the RC frame, the experimental investigation in this study encompassed various activities. In particular, a quasi-static cyclic loading procedure was executed on the RC frame. Specifically, to replicate a seismic action, a sequence of increasing-amplitude, quasi-static cyclic displacements D was applied at the upper free end “C” of the column. The adopted loading sequence shown in Figure 4 consisted of several sets of displacements aiming to produce progressive damage on frame elements. Each set comprised three fully reversed identical cycles. No axial load was applied to the column in direction “CB”, thus reducing any positive influence on the shear capacity of the joint [34].

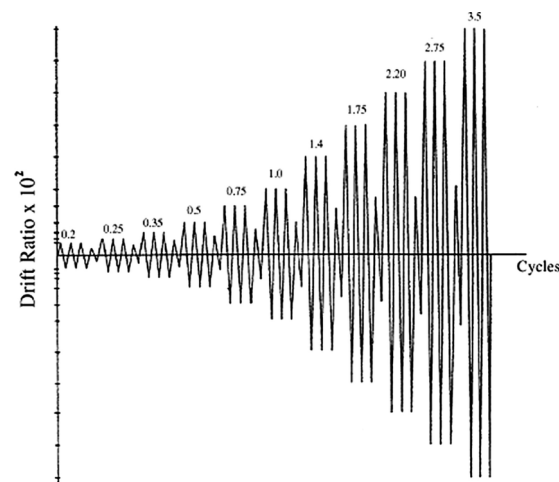


Figure 4. Ideal standard test protocol ACI 374.1 (2005).

The resulting hysteresis cycles obtained from the test are depicted in Figure 5 in terms of the shear force T resisted by the frame with respect of the imposed displacement D . In the same graph, some of the hysteresis cycles are numbered to later compare the experimental results with those obtained from the numerical analysis (see Section 5).

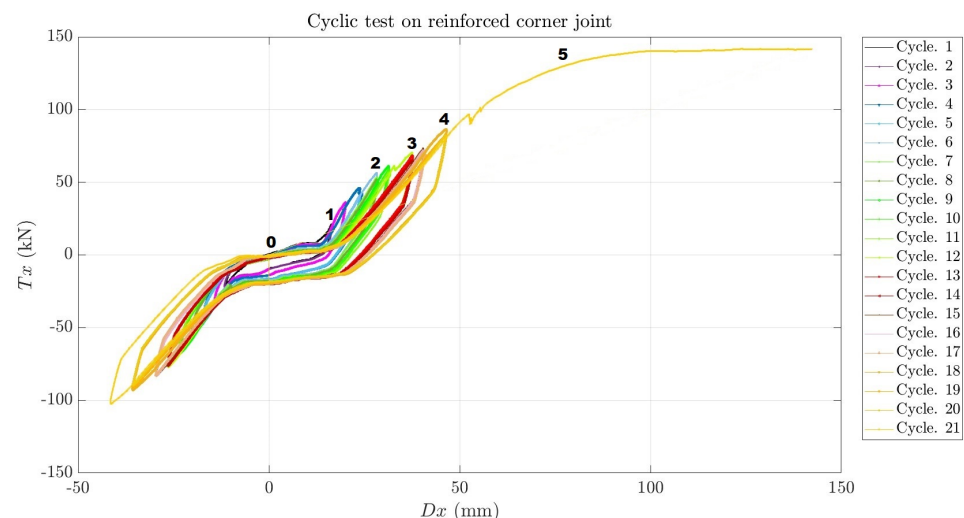


Figure 5. Experimental data of forces and displacements recorded during the cyclic loading. Numeration of the AVT measurements.

At the end of the specific set of cycles (those numbered in Figure 5), and thus, at various stages of the frame progressive damage, ambient vibration tests (AVTs) were performed before restarting with subsequent groups of cycles. In particular, Figure 6a depicts the quasi-static test setup configuration, showcasing the positioning of the loading point, of the constraints applied to the RC frame, and of the 6 accelerometers. Ambient vibration tests (AVTs) were conducted using a “hammer” to activate vibrations in the frame.

The stages of damage selected for performing the AVT were established based on the maximum displacement values achieved during the quasi-static tests. For each ambient vibration test, the acquisition duration was approximately 10 min, with a sampling frequency of 200 Hz.

By coupling the outcomes derived from the quasi-static tests with those from the ambient vibration tests, an investigation was made of the progressive damage in the RC frame. More specifically, the investigation focused on the interplay between the changes in the modal parameters and the reduction in the frame’s stiffness due to the incremental cyclic loading.

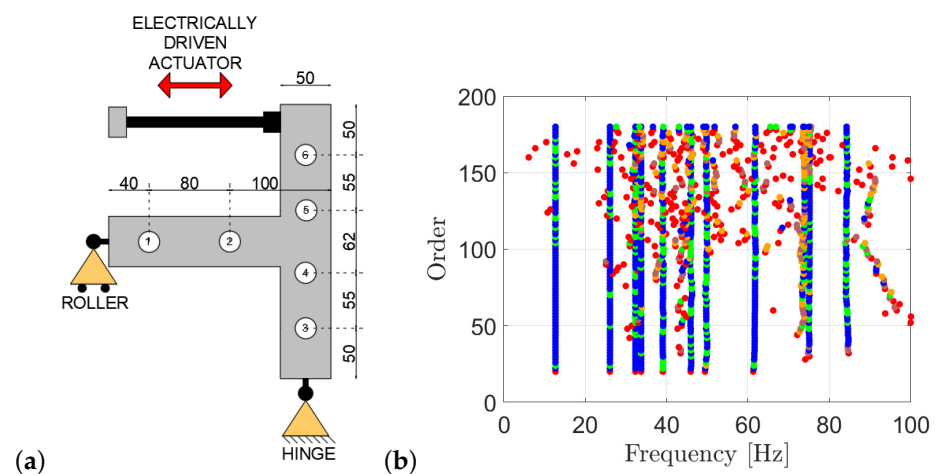


Figure 6. (a) AVT experimental setup; (b) stabilization diagram referring to stage 0 (undamaged stage of the specimen).

Later, data collected from both the quasi-static and the ambient vibration tests underwent processing using the stochastic subspace identification covariance-driven (SSI-cov) from [35]. Widely acknowledged for its effectiveness in extracting modal parameters from measured data, this algorithm was implemented using the open-source software PyOMA [36].

Figure 6b shows the stabilization diagram generated by applying the SSI-cov algorithm to the data associated with the undamaged state of the RC frame. The stabilization diagram gives a visual representation of the identified modal parameters as a function of the model order.

In actuality, the high-quality estimation of approximately seven modes within the frequency range of 0 to 100 Hz was achieved. These modes encapsulate the intrinsic and reference vibration characteristics of the RC frame, offering invaluable insights into its dynamic behavior. The precise estimation of the modal parameters held a pivotal role in comprehending the structural response, and subsequently, analyzing the impact of progressive damage on the RC frame.

Figure 7 presents a 2D depiction of the experimental modal shapes during the undamaged phase. It aids in comprehending the distortion of the T-shaped element within the same plane as the external forces. The dashed line represents the frame’s undeformed configuration, while the solid line represents the i -th modal shape.

Figure 7 effectively displays the overlay of the plan view of the undeformed joint and its corresponding modal deformation. In terms of the classification between the translational and rotational modes, it was indeed challenging to make a clear distinction.

A translational mode should be understood as one with a predominant translational deformation, and a torsional mode as one with a predominant rotational deformation. It can be observed that both the first and fourth modes exhibited significant deformation components, with the branches of the joint showing a clear deformation field due to their mutual rotation. In the other modes, a predominant translational component was manifested despite the presence of deformation along the longer branch of the joint.

In Figure 7, only the positions of the six accelerometers are illustrated (not the entire frame's geometry). The first mode, which was distinguished by a reference frequency of 24.04 Hz, showcased the most pronounced distortion of the joint.

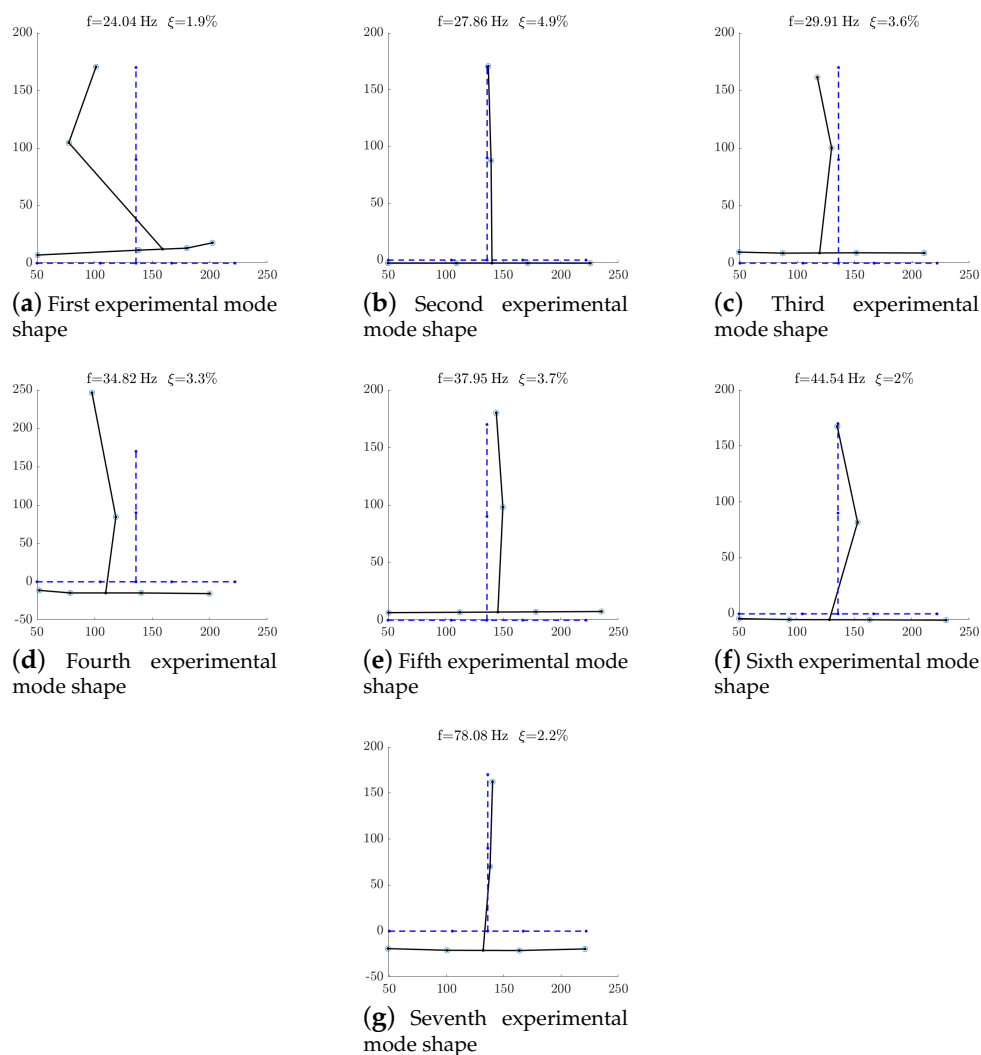


Figure 7. Two-dimensional representation of the first seven experimental mode shapes corresponding to the undamaged stage of the specimen.

4. Analysis of Experimental Results

From the loading test, capacity curves were generated for each cycle. These curves allowed for the determination of the stiffness factor K . In particular, this factor was calculated as the ratio between the shear force (T_x) and the corresponding displacement (Dx), with both measured at the peak of the considered cycle.

More specifically, Dx denotes the maximum displacement applied to the column end "C" during the i -th cycle, while T_x is the corresponding measured force. The K factor is indicative of the system's stiffness, and visually represents the tangent of the angle α

formed by the line connecting the curve's peak with the origin of the axes with respect to the x-axis. This graphical representation is demonstrated in Figure 8a.

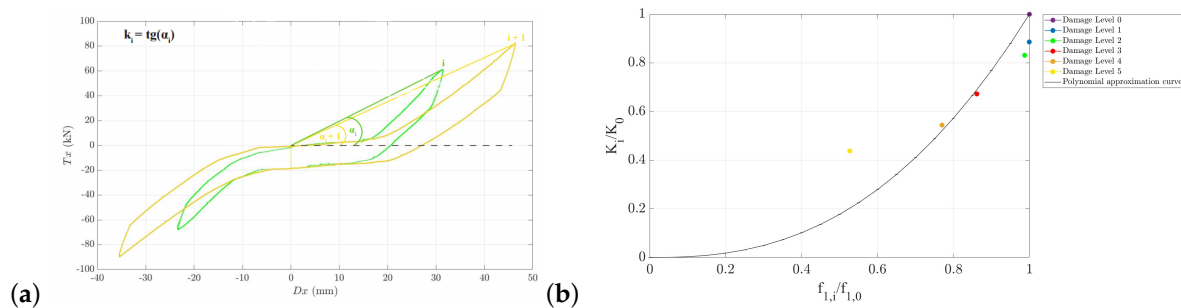


Figure 8. (a) Graphical meaning of the stiffness factor $K = \tan(\alpha_i)$; (b) relationship between the decay in stiffness K_i/K_0 and the variation in the first modal frequency $f_{1,i}/f_{1,0}$.

Out of the total 21 cycles conducted (7 groups of 3 cycles each), emphasis was placed on those 6 after which the AVT was carried out and the accelerometer measurements were taken. Please note that the first of the six AVT measurements was recorded at stage 0, which corresponded to the undamaged condition of the specimen (before performing the loading test; also see Figure 5). The resulting K values obtained from these cycles are presented in Table 2.

Table 2. Stiffness values, natural frequencies, and damping values estimated for the undamaged stage (0) and for the subsequent five damage levels.

	Damage Level					
	0 (Ref.)	1	2	3	4	5
D_x	12.59	28.3	37.52	48.46	70.49	143.29
T_x	28.41	56.6	70.4	73.56	86.59	141.73
k	2.257	2.00	1.876	1.518	1.228	0.989
f_1	24.04	24.03	23.74	20.71	18.51	12.67
f_2	27.86	32.59	33.43	31.29	19.61	26.07
f_3	29.91	37.38	39.25	39.86	32.74	32.35
f_4	34.82	49.21	42.20	49.34	40.00	33.32
f_5	37.95	50.25	50.10	50.60	42.59	39.18
f_6	44.54	52.68	52.26	55.35	52.27	46.00
f_7	78.08	65.58	65.39	79.81	64.89	75.01
ζ_1	1.85	1.54	1.17	1.29	2.38	0.50
ζ_2	4.92	4.55	1.31	3.09	2.18	0.89
ζ_3	3.60	2.96	0.61	1.61	1.29	0.62
ζ_4	3.26	1.39	4.39	2.16	2.63	2.69
ζ_5	3.72	3.92	1.32	2.22	2.44	2.45
ζ_6	2.02	1.55	2.26	1.89	0.40	1.21
ζ_7	2.17	1.77	1.99	0.93	1.49	2.02

The decrease in stiffness, as indicated by variations in the parameter K , highlights the stiffness loss that resulted from the progressive damage induced by cyclic loading. In reality, as the number of cycles increased, the joint and the other frame elements underwent an increasing number of cracks (also growing in width), which produced a reduction in the stiffness results.

Consequently, changes in the natural frequencies of the frame were also recorded. As said in the previous Section 4, frequencies were assessed at six levels of damage and the final results are reported in Table 2.

Please note that Table 2 is not a MAC (modal assurance criterion) matrix, which typically exhibits similarity in its diagonal elements. Instead, it simply illustrates the evolution

of selected parameters (such as stiffness and frequency) at each step of the degradation process. Consequently, there is no requirement for similarity in the diagonal elements.

The data in Table 2 allow for a comparative analysis between the measured dynamic parameters, offering insights into the relationship between the structural damage and the dynamic response of the specimen.

For each damage level, the table lists the values of the first seven natural frequencies of the frame in hertz (Hz). Because each natural frequency represents the inherent frequency at which the structure tended to vibrate when excited, it may serve as a crucial indicator of the frame's structural response, mostly in terms of the its stiffness characteristics. In fact, as the damage level progressed, noticeable changes in the natural frequencies were measured. For instance, at damage level 1, there was a slight increase in f_2 , while at damage level 4, a significant reduction was observed in f_7 compared with the undamaged phase (0). These variations highlight the impact of damage on the structural dynamic properties of the tested frame.

In addition to the natural frequencies, the table presents the damping values (ζ_1 to ζ_7) associated with each damage level. Damping reflects the energy dissipation capability of the structure and affects the decay rate of vibration amplitudes. Changes in damping values signify alterations in the structure's energy dissipation behavior due to damage. Notably, there were fluctuations in the damping values across different damage levels. For instance, at damage level 4, ζ_3 exhibited a higher damping ratio compared with the undamaged phase, indicating an increase in energy dissipation.

The analysis of results reported in Table 2 allowed for a better understanding of the structural response and its evolution as damage accumulated. The variations observed in these parameters offer insights into the progressive degradation of the RC frame and aid in the assessment of its structural integrity.

In Table 3, the modal assurance criterion (MAC) is shown with a color code. The MAC is a classical metric introduced by Allemang and Brown in 1982 to compare mode shapes and assess their similarity. It is among the most used metrics in modal tracking approaches. Therefore, the authors implemented MAC calculations to compare the mode shapes estimated at each step of the degradation process of the joint.

These results were obtained by comparing the modes estimated in two consecutive stages, namely, states 0-1, 1-2, 2-3, 3-4, and 4-5. The MAC was calculated as follows:

$$\text{MAC} = (\phi_r, \phi_s) = \frac{|\phi_r \cdot \phi_s^T|^2}{(\phi_r \cdot \phi_r^T)(\phi_s \cdot \phi_s^T)} \quad (1)$$

where the operator “ \cdot ” stands for the inner product, ϕ_r represents the experimental mode shape, and ϕ_s indicates the numerical mode shapes.

Each cell in the table represents the MAC value computed between the modes of the corresponding states. The diagonal elements of the table represent the similarity of modes within the same state (state 0 to state 0, state 1 to state 1, and so on).

The off-diagonal elements of the table represent the similarities between modes of different states. For example, the cell at the intersection of state 1 and state 0 represents the MAC value between the modes of state 1 and state 0. Similarly, the cell at the intersection of state 4 and state 5 represents the MAC value between the modes of state 4 and state 5.

MAC values range from 0 to 1, with 1 indicating a perfect match between the experimental and the numerical mode and 0 indicating no similarity.

The main aspects that arose from the observation of the experimental data summarized in Tables 2 and 3 were as follows:

- Modal tracking was challenging due to progressive damage within the RC joint, resulting in low MAC values for mode shape comparison.
- The initial modes experienced a significant reduction in natural frequency due to the distortion mode of the T-element, which was highly affected by the stiffness reduction caused by damage (from 24.04 Hz to 12.67 Hz).

- Higher modes showed little in-plane deformation of the T-element, as reflected in their natural frequencies being almost independent of the damage level. However, the natural frequency of the last mode paradoxically increased from 81 Hz to 84 Hz, possibly due to boundary condition variations in the final damage phase.

Table 3. Representation of the MAC matrices. Each sub-table shows the MAC computed between the modes of two consecutive stages.

		State 0							State 3								
State 1		0.00	0.02	0.02	0.01	0.00	0.00	0.58	State 4		0.64	0.39	0.69	0.46	0.08	0.00	0.12
		0.13	0.77	0.70	0.01	0.50	0.04	0.02			0.01	0.06	0.01	0.10	0.01	0.02	0.15
		0.17	0.27	0.24	0.02	0.00	0.01	0.47			0.00	0.00	0.00	0.05	0.02	0.02	0.02
		0.08	0.47	0.45	0.00	0.38	0.02	0.00			0.45	0.35	0.46	0.18	0.20	0.01	0.29
		0.04	0.16	0.23	0.25	0.00	0.07	0.23			0.21	0.11	0.20	0.21	0.11	0.06	0.34
		0.58	0.04	0.06	0.71	0.05	0.78	0.14			0.05	0.12	0.04	0.02	0.02	0.04	0.25
		0.31	0.03	0.05	0.57	0.01	0.19	0.40			0.09	0.21	0.03	0.06	0.38	0.00	0.00
		State 1							State 4								
State 2		0.00	0.02	0.02	0.01	0.00	0.00	0.58	State 5		0.99	0.56	0.75	0.15	0.08	0.08	0.43
		0.13	0.77	0.70	0.01	0.50	0.04	0.02			0.90	0.45	0.81	0.17	0.13	0.23	0.30
		0.17	0.27	0.24	0.02	0.00	0.01	0.47			0.93	0.47	0.62	0.14	0.04	0.03	0.43
		0.08	0.47	0.45	0.00	0.38	0.02	0.00			0.26	0.26	0.08	0.01	0.01	0.11	0.21
		0.04	0.16	0.23	0.25	0.00	0.07	0.23			0.28	0.02	0.08	0.04	0.23	0.29	0.21
		0.58	0.04	0.06	0.71	0.05	0.78	0.14			0.01	0.26	0.07	0.00	0.00	0.00	0.01
		0.31	0.03	0.05	0.57	0.01	0.19	0.40			0.15	0.00	0.06	1.00	0.30	0.01	0.27
		State 2															
State 3		0.10	0.19	0.17	0.07	0.13	0.01	0.09									
		0.28	0.00	0.00	0.99	0.47	0.01	0.02									
		0.27	0.00	0.00	0.97	0.51	0.00	0.03									
		0.00	0.00	0.14	0.04	0.00	0.03	0.10									
		0.21	0.17	0.04	0.28	0.01	0.24	0.12									
		0.02	0.08	0.18	0.00	0.08	0.04	0.01									
		0.03	0.09	0.00	0.01	0.02	0.29	0.73									

The first mode, as seen in Figure 7, had the most pronounced distortion of the joint, and this is precisely why it was singled out among the various other modes; it was chosen to investigate a relationship between alterations in the frame's dynamic response and the accumulation of structural damage during the cyclic loading of the frame.

According to this assumption, the graph in Figure 8b highlights a relationship between the residual stiffness K_i at the damage stage i , which was normalized with respect to the undamaged level K_0 (as obtained from the experimental cyclic load test), and the residual frequency $f_{1,i}$ of the first mode at stage i (measured using the ambient vibration test), which was normalized with reference to the undamaged stage frequency $f_{1,0}$. The polynomial approximation, expressed by the equation

$$K = 0.9913f^{1.9933} \quad (2)$$

fit the experimental data well, with $R^2 = 0.9478$.

Actually, the graph depicted in Figure 8b illustrates how the system's progressive damage due to cyclic displacements resulted in a gradual reduction in both the frame stiffness and its first natural frequency.

5. Numerical Analysis

5.1. Numerical Models and Results

Alongside the experimental dynamic and mechanical characterization of the tested "RC frame", several finite element models (FEMs) of the specimen were built and analyzed to better understand the relationship between the changing dynamic behavior of the RC frame with respect to the progressive structural damage induced by the cyclic loads.

In particular, numerical analyses were conducted to closely replicate the experimental setup and to determine the system's first natural frequency at each stage of the progressive damage. To simulate the progressive damage, Young's modulus E was made to vary in different parts of the modeled structure. In particular, six stages of damage were simulated by reducing the Young's modulus from 0% to 80% of its initial reference value $E_0 = 30,373$ MPa.

Details about the FEMs considered in this section of the work are illustrated in Figure 9. In particular, to replicate the strut and tie mechanism that took place in the RC joint, it was modeled using two diagonal connecting rods with hinges at the ends. Concerning the main beam "BG" and the two half-columns "1-6" and "8-A", they were modeled as frame elements, with each divided into five segments. A roller was modeled at the right end of the beam, while a hinge was introduced at the lower end of the column. As already said, the E values assigned to each segment of the structure were gradually reduced, starting from undamaged stage 0 (the reference stage, representing an intact system) through to damage stage 5. In order to better comprehend the observed experimental progressive damage suffered by the real frame and to investigate the impacts of different types of damage on the reduction in the total system's natural frequency, seven FEMs of the frame were analyzed, with each varying in terms of the element affected by the damage. The considered FEMs are listed as follows:

- Model "J": only the joint was progressively damaged.
- Model "C": only the column was progressively damaged.
- Model "CJ": both the joint and column were progressively damaged.
- Model "B": only the beam was progressively damaged.
- Model "BJ": both the joint and beam were progressively damaged.
- Model "BC": both the column and beam were progressively damaged.
- Model "BCJ": all elements of the system were progressively damaged.

Please note that the FEM names are acronyms that indicate the specific frame part that was affected by the progressive damage to help with establishing a consistent model nomenclature.

For example, schemes (a), (b), and (c) of Figure 9 show how the models from B0 to B2 were made. In particular, model B0 was equal to models J0, C0, CJ0, BJ0, BC, and BCJ0 since they all corresponded to damage stage 0, in which the whole system was undamaged. Then, model B1 was thought to represent structural damage starting in the beam and near the joint, and thus, E_1 was assigned to segment "BC", where bending moment M and shear forces T were higher for the beam; the other beam's segments ("CD", "DE", "EF", "FG") were considered undamaged and E_0 was assumed for them. Therefore, in the FEM B2, a higher beam damage was modeled by assigning a more reduced value E_2 to segment "BC" (near the joint), assigning E_1 to the subsequent segment "CD", and assuming the rest of the beam was undamaged with $E = E_0$ (Figure 9c). In so doing, the beam presented progressively more important damage near the joint and gradually less damage as the distance from the joint increased. This was until case B5, where the damage near the joint was assumed to be at the maximum level (E_5 was assigned to the segment "BC") and the minimum damage was at the final segment of the beam (with E_1 assigned to segment "FG"). Moving from segment "BC" (near to the joint) to segment "FG" (at the end of the beam), progressively decreasing values of E were assigned. Similar assignments were undertaken for all the models listed above, and FEM referred to damage stages 0, 1, and 2 of model CJ are shown as examples in Figure 9d, e, and f, respectively.

In Table 4, the ratio $f_{1,i}/f_{1,0}$ between the calculated first natural frequency of the considered model at its damage stage i (named $f_{1,i}$) and the value of the first natural frequency of the same considered model at its undamaged stage (named $f_{1,0}$, reference value) are reported.

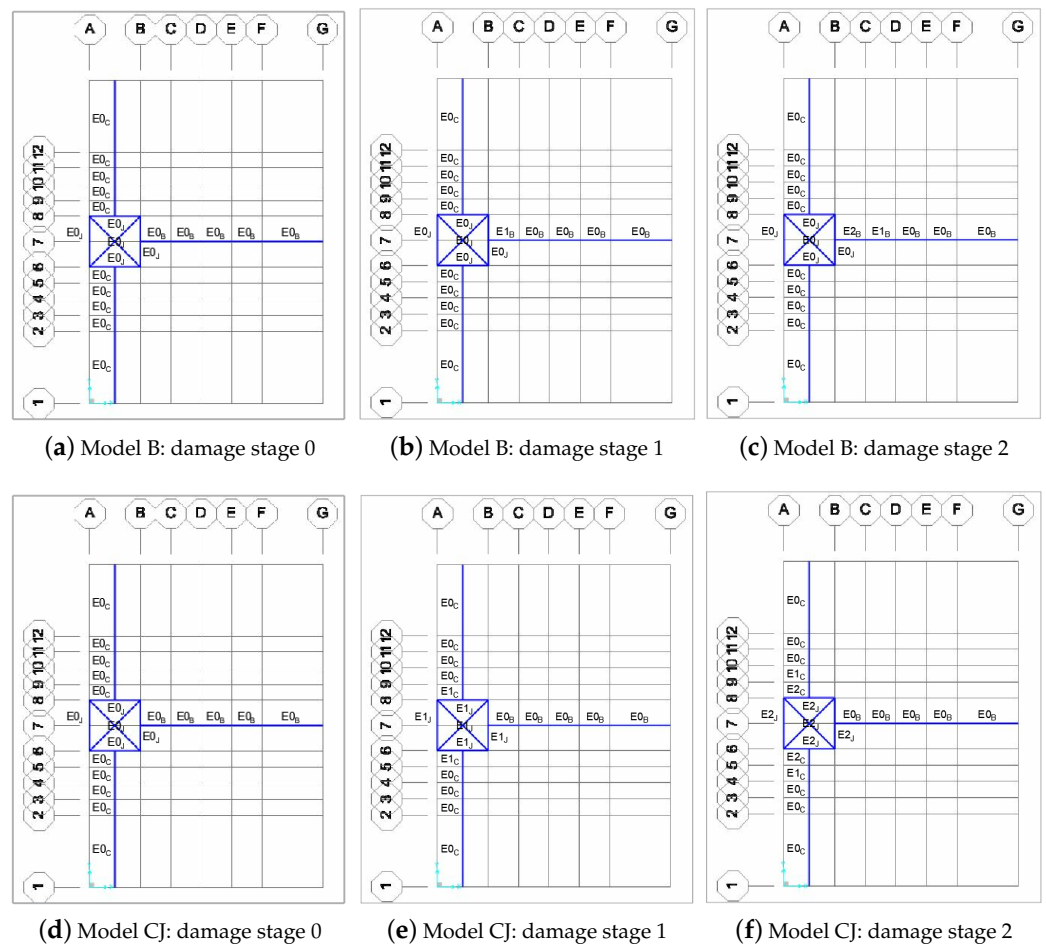


Figure 9. (a–c) Stages of the progressive damage considered in model “B”: only the main beam was affected by the progressive damage; (d–f) stages of the progressive damage considered in model “CJ”: both the column and the joint were affected by the progressive damage.

In the same table, the ratio K_i/K_0 between the stiffness of the considered model at its stage i (named K_i) and the value of the stiffness of the same considered model at its undamaged stage (named K_0 , reference value) are also reported.

The data in Table 4 show that the relationship between the frequency decay and stiffness decay depended on the type of damage location. In particular, the frequency decay was faster in the case of the damage localized on the beam than in the case of damage localized only on the joint. Obviously, the worst case was the one with the damage localized simultaneously on the beam, column, and joint.

As already done in the previous Section 4 (with respect to the natural frequency of the system experimentally measured through the AVT), in this section of the paper, a correlation is considered between values of the first natural frequency and stiffness values calculated for the frame at various damage stages through the numerical analysis of the FEMs described in this section. In particular, the data of Table 4 are plotted in the graph of Figure 10, which represents how the values of the residual frequency $f_{1,i}/f_{1,0}$ related to the calculated values of the residual stiffness K_i/K_0 of the system with the indication of the various damage stages.

All the curves depicted in Figure 10 highlight a nonlinear decay of the first natural frequency of the system as a result of the increasing structural damage suffered by the frame. The results define a range of minimum and maximum values within which the natural frequency of the system could vary when the distribution of stiffness across the frame components also changed. For example, in Figure 10, it is shown that a reduction to 40% of

the original stiffness of the structure ($K_i/K_0 = 0.4$) could result from a variety of different damage distributions (from damage model J to damage model BCJ), also highlighting that different residual natural frequencies (ranging from 62% to 92% of the value corresponding to the undamaged stage) may correspond to the same structural health condition for the structure (here represented by a residual stiffness fixed to 40% of the initial one). The graph also shows that a given frequency reduction (for example, $f_{1,i}/f_{1,0} = 0.92$) could result from a high-damage stage in the joint (damage stage 4), as well as from a lower damage stage in the beam (damage stage 2) instead.

Table 4. Residual values of the first natural frequency and of the residual stiffness, which were calculated for each of the six damaged stages for each of the seven considered models.

	Models						
	J	C	CJ	B	BJ	BC	BCJ
$f_{1,0}/f_{1,0}$	1	1	1	1	1	1	1
$f_{1,1}/f_{1,0}$	0.986	0.979	0.966	0.965	0.952	0.904	0.894
$f_{1,2}/f_{1,0}$	0.976	0.965	0.944	0.922	0.903	0.851	0.836
$f_{1,3}/f_{1,0}$	0.947	0.923	0.881	0.841	0.810	0.727	0.707
$f_{1,4}/f_{1,0}$	0.924	0.890	0.836	0.764	0.729	0.654	0.632
$f_{1,5}/f_{1,0}$	0.829	0.759	0.680	0.655	0.624	0.583	0.447
K_0/K_0	1	1	1	1	1	1	1
K_1/K_0	0.8	0.8	0.8	0.8	0.8	0.8	0.8
K_2/K_0	0.7	0.7	0.7	0.7	0.7	0.7	0.7
K_3/K_0	0.5	0.5	0.5	0.5	0.5	0.5	0.5
K_4/K_0	0.4	0.4	0.4	0.4	0.4	0.4	0.4
K_5/K_0	0.2	0.2	0.2	0.2	0.2	0.2	0.2

Thus, these considerations make it clear that, unfortunately, a nonunivocal relationship should always be expected between the natural frequency variation detected with the AVT and the type and level of the damages actually suffered by an RC frame.

In addition, it must also be noticed that in this experiment, the first natural frequency decay did not depend on the material properties (which were constant during the test), but rather on the distribution of stiffness throughout the structural system (which changed due to the progressive structural damage).

As was already said, the seven models analyzed in this study differed from each other in terms of the type and number of structural elements (beam, column, joint) subject to the damage. In each model, Young's modulus was gradually reduced in the damaged parts to evaluate their influence on the decay of the first natural frequency of the frame. The computed frequency variations are reported in Table 4.

The curves in Figure 10 also highlight that, among all cases, the damage in the beam had the most significant influence on the frame frequency, while damage in the joint had less impact. Consequently, it can be asserted that employing natural frequency monitoring to evaluate whether the beam–column joint is undergoing cracking may be less effective than actually expected. Conversely, frequency monitoring may be very sensitive in detecting the structural health of a beam, namely, the element predominantly influenced the variation in the system's natural frequencies. Because during the experimental test, cracks were noticed in the joint (primarily), as well as in the beam and in the column, experimental variation in the natural frequency resulted from different damage processes all took place at the same time.

In fact, for lower damage levels, when the system's stiffness remained considerable, the experimental values remained close to the model J curve, which was the joint where the frame part was actually damaged first. In other words, this similarity between the first experimental data and the model J scenario was consistent with expectations, whereas in the first part of the experiment, structural damage took place in the joint.

As the damage intensified, the experimental values correctly shifted toward models BC and BCJ, where damage in the beam was modeled. Actually, due to the specific test setup, the beam experienced a higher bending moment M and shear forces T compared with the column, although these elements were both characterized by equivalent strength.

Thus, it was established that in the case of the RC frame, monitoring the natural frequencies of the system may be relatively effective in assessing the beam's health condition and less promising in tracking the joint damage evolution.

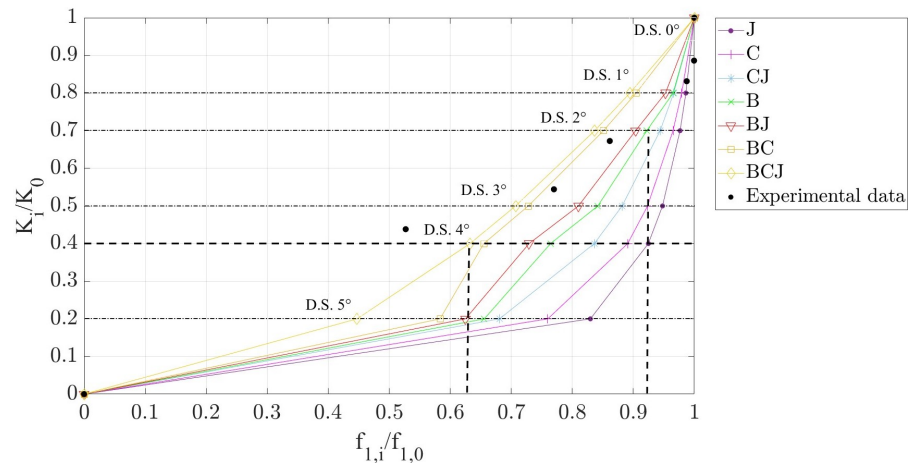


Figure 10. Relationship between residual stiffness (K_i/K_0) and residual frequency ($f_{1,i}/f_{1,0}$) resulting from the analysis of the FEMs (six damage levels for each of the seven models) and comparison with the numerical models.

5.2. Additional Consideration

It must be observed that in the case of monitoring existing structures (buildings, bridges, etc.), the stiffness value K_0 referring to the undamaged stage of the structure is often unknown, and this value is conceptually associated with the time t_0 at which the structure experienced the first load. For this reason, only the current stiffness K_0^* of the structure at the beginning of the survey can be assumed as the reference stiffness for the comparison with the stiffness measurements repeated at different times in the future.

Similarly, in the case of structures already in service, only the current first natural frequency of the structure at the beginning of the survey can be assumed as the reference frequency f_0^* and compared with values of the first natural frequency measured subsequently.

In accordance with these considerations resulting from numerical simulations carried out in this study, one may assume the damage stage $i-1$ to be the reference in comparison with damage stage i . In so doing, residual values of the stiffness K_i and of the first natural frequency f_i were normalized with respect of their values at the previous steps K_{i-1} and $f_{1,i-1}$, respectively, and are plotted in Figure 11.

The graph in Figure 11 also shows the data related to the experimental damage history. Since, as noted above, there is no biunivocal correlation between the AVT measurements and damage stages, and the same happened between changes in the stiffness and the type of damage, the graph in Figure 11 shows that only by intersecting information about frequency changes and changes in stiffness, it was possible to determine the type and level of damage that affected the structure. In other words, it is recommended to contemporarily measure changes in natural frequencies with AVT techniques and changes in structural stiffness with static load tests, and to repeat this procedure during the life of the structure to understand whether its damage grows according to diffuse or localized damage models. For example, the experimental data in the graph of Figure 11 show that during the cyclic tests, the damage occurred in a diffuse way and was not localized only in the joint, as might have been expected from the test design (in fact, the experimental damage was close to the BCJ curve and not to the J curve).

In so doing, curves already plotted in the previous Figure 10 were recalculated to attempt to search for a mathematical correlation between the residual structural stiffness values and the residual values of the first natural frequency of the system.

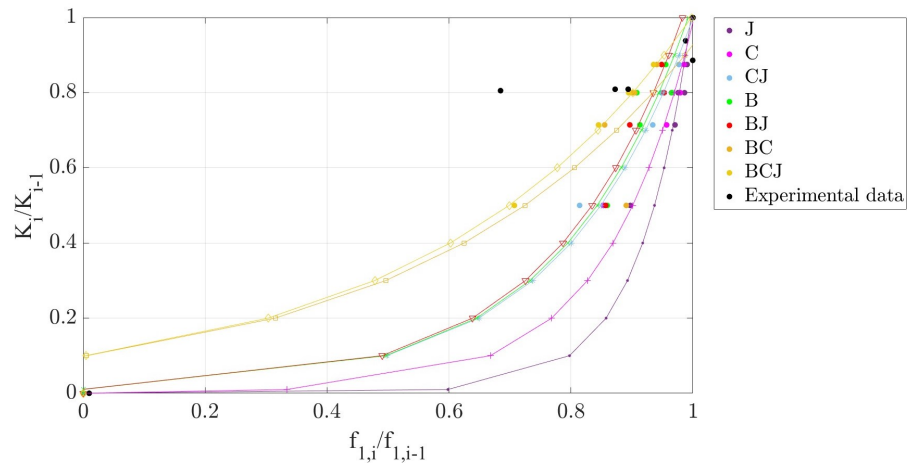


Figure 11. Relationship between calculated residual normalized stiffness values K_i/K_{i-1} and calculated residual normalized frequency values $f_{1,i}/f_{1,i-1}$: exponential approximation curves.

5.3. Numerical Regression and Errors

Exponential, parabolic, and logarithmic approximation curves were generated and their equations, along with their coefficients of determination (R^2), were calculated and are summarized in the following Table 5 with respect to the experimental data of $f_{1,i}/f_{1,i-1}$ and K_i/K_{i-1} . As an example, the following Figure 11 shows the exponential approximation curves for the seven models studied in the previous Section 4.

Table 5. Coefficients of the equations of the approximation curves and their coefficients of determination R^2 .

Model	Polynomial Approximation Curves									
	Exponential Approximation [$y = ae^{(bx)}$]			Parabolic Approximation [$y = ax^2 + bx + c$]				Logarithmic Approximation [$y = bln(x) + c$]		
	a	b	R^2	a	b	c	R^2	b	c	R^2
J	0.00001	11.548	0.9527	-1.4515	2.4089	0.0065	0.9934	0.1998	1.0231	0.9984
C	0.001	6.8954	0.9699	-1.3184	2.2873	0.0041	0.9963	0.1979	1.0098	0.9987
CJ	0.0102	4.5845	0.9874	-1.1815	2.1565	0.003	0.9974	0.195	0.9931	0.9962
B	0.01	4.6407	0.9601	-1.2512	2.1953	0.0095	0.9858	0.1922	0.9851	0.9960
BJ	0.0101	4.6756	0.9538	-1.2148	2.154	0.0107	0.9832	0.1905	0.9769	0.9959
BC	0.0987	2.2396	0.8767	-1.2175	2.1334	0.0169	0.9656	0.1872	0.9649	0.9873
BCJ	0.099	2.3181	0.9991	-0.7538	1.7322	0.003	0.9979	0.1838	0.9312	0.9723

As can be seen from Figure 11, comparing K_i with the stiffness values K_{i-1} calculated at the previous damage level, a difference in frequency decay was made explicit for each of the seven models considered to describe the progressive damage in different parts of the frame: again, the natural frequency of the whole frame primarily depended on the health condition (damage level) of the beam and less on the joint health condition.

Additionally, from Table 5, it can be seen that although some approximation curves had a high R^2 , other types of regression may better fit the calculated data. This was made clearer by the values of four additional error indexes considered in this study to assess which type of regression best approximated the experimental results. These indexes were the MSE (mean squared error), RMSE (root-mean-squared error), MAE (mean absolute error), and MAPE (mean absolute percentage error), and for all of them, the lower the value, the better the quality of the considered regression law. In Table 6, the values of all the abovementioned indexes calculated for all the data regression laws are summarized. From them, it can be seen that the curves that best approximated the results were the parabolic and logarithmic ones, with their errors being the lowest among all curves.

Table 6. Other error indexes calculated for the parabolic, exponential, and logarithmic approximation curves.

Other Error Indexes of the Polynomial Approximation Curves												
Model	Parabolic Approximation				Logarithmic Approximation				Exponential Approximation			
	MSE	RMSE	MAE	MAPE	MSE	RMSE	MAE	MAPE	MSE	RMSE	MAE	MAPE
J	0.00067	0.025	0.020	2.21	0.0012	0.035	0.021	2.11	0.12	0.033	0.015	1.71
C	0.00036	0.019	0.015	1.63	0.0022	0.047	0.024	2.51	0.0023	0.048	0.025	2.85
CJ	0.00025	0.015	0.012	1.35	0.0031	0.056	0.027	2.89	0.0033	0.057	0.030	3.59
B	0.0014	0.037	0.027	3.09	0.0016	0.040	0.028	3.04	0.0017	0.042	0.030	3.42
BJ	0.0016	0.040	0.030	3.43	0.0015	0.039	0.028	3.06	0.0016	0.040	0.030	3.43
BC	0.0033	0.058	0.045	5.08	0.0013	0.037	0.029	3.20	0.0034	0.058	0.051	5.78
BCJ	0.00018	0.013	0.011	1.38	0.0061	0.078	0.044	4.92	0.0077	0.088	0.059	7.64

6. Conclusions and Remarks

An experimental campaign was carried out to investigate the effectiveness of the AVT for structural health monitoring of an RC frame subject to extreme cyclic loading. Both quasi-static testing and repeated OMA were performed to describe the damage evolution in the frame.

The quasi-static test on the RC frame consisted of seven groups of three cycles performed at increasing values of displacements (seven levels of structural damage). At the end of each group, the modal frequencies of the frame were assessed by the ambient vibration test (AVT).

The experimental tests revealed the modes associated with a significant distortion component to exhibit a clear reduction in the associate frequency, indicating a loss in stiffness for the RC frame.

At the same time, the modal tracking was found to be challenging due to significant variations in the mode shapes across different damage stages. Substantial changes in mode shapes resulted in low modal assurance criterion (MAC) values, which made it difficult to determine the correspondence between modes at different stages of the damage progression. The first mode frequency showed a significant reduction, becoming an interesting indicator of the stiffness variations for the analyzed structural system. A clear correlation between the experimental values of the residual first mode frequency (assessed through the AVT) and the experimental values of the residual stiffness during the cyclic loading of the frame were highlighted.

The same correlation was investigated through numerical analysis as well. In particular, various FEMs of the tested RC frame were analyzed to reproduce different types and distributions of structural damage: damage in the joint only (J), in the beam only (B), in the column only (C), and several combinations of the previous scenarios.

The results of the experimental test show that the experimental first natural frequency decreased by 47.3% from stage 0 (undamaged) to stage 5; the experimental stiffness decreased by 56.18% from stage 0 (undamaged) to stage 5. In addition, the results of the numerical analysis show that the damage of the beam had a greater influence on the variation of f than either the column or the joint (Table 7).

Table 7. Variation in the first natural frequency of the numerical models between undamaged stage 0 and stage 5.

	Models							
	J	C	CJ	B	BJ	BC	BCJ	
$f_{1,0}/f_{1,5}$	17.1%	24.1%	32%	34.5%	37.6%	41.7%	55.3%	

A clear nonlinear relationship between the calculated values of the first mode frequency and the frame stiffness at various stages of the structural damage evolution were identified with respect of each type of damage distribution.

The decay of the residual frequency of the system was found to depend on the type of damage distribution considered. In particular, the analyses showed that the damage in the

beam had a much greater impact on the frame stiffness compared with damage that took place in the joint only.

Consequently, using the AVT to assess the structural health of a beam column joint may not be as effective as actually expected if the joint is undergoing a strong reduction in stiffness due to intense cracking. Conversely, the AVT and frequency monitoring may be very sensitive when detecting the structural health of the beam, namely, the element predominantly influencing the variation in the system's natural frequencies.

In conclusion, the AVT was found to have interesting potential in investigating the progressive damage that takes place in RC frames under extreme cyclic loads, especially when it is carried out in combination with static tests for the direct measurement of the structural stiffness variation. In so doing, the type, level, and distribution of progressive structural damage may be successfully investigated.

Author Contributions: Conceptualization, A.G.; methodology, A.G., L.B., R.C. and R.A.; validation, A.G.; formal analysis, A.G., L.B., C.D. and A.A.; investigation, A.G., L.B., C.D. and A.A.; data curation, A.G., L.B., C.D., A.A., R.C. and R.A.; writing—original draft, A.G., L.B., C.D., A.A., R.C. and R.A.; writing—review and editing, A.G., L.B., C.D., A.A., R.C. and R.A.; visualization, A.G., L.B., C.D. and A.A.; supervision, A.G.; project administration, A.G.; funding acquisition, A.G. All authors read and agreed to the published version of the manuscript.

Funding: This work was carried out as part of the DPC-ReLUIIS 2022–2024 research project funded by the Department of Civil Protection.

Data Availability Statement: The data used to support the findings of this study are available from the corresponding author upon reasonable request.

Acknowledgments: The authors would like to thank the anonymous reviewers for their valuable comments and suggestions in revising the paper.

Conflicts of Interest: The authors declare no conflicts of interest.

References

- Huang, H.; Guo, M.; Zhang, W.; Zeng, J.; Yang, K.; Bai, H. Numerical investigation on the bearing capacity of RC columns strengthened by HPFL-BSP under combined loadings. *J. Build. Eng.* **2021**, *39*, 102266. [\[CrossRef\]](#)
- De Risi, M.T.; Ricci, P.; Verderame, G.M.; Manfredi, G. Experimental assessment of unreinforced exterior beam–column joints with deformed bars. *Eng. Struct.* **2016**, *112*, 215–232. [\[CrossRef\]](#)
- Calvi, G.M.; Magenes, G.; Pampanin, S. Relevance of beam-column joint damage and collapse in RC frame assessment. *J. Earthq. Eng.* **2002**, *6*, 75–100. [\[CrossRef\]](#)
- Wei, J.; Ying, H.; Yang, Y.; Zhang, W.; Yuan, H.; Zhou, J. Seismic performance of concrete-filled steel tubular composite columns with ultra high performance concrete plates. *Eng. Struct.* **2023**, *278*, 115500. [\[CrossRef\]](#)
- Masi, A.; Santarsiero, G. Seismic tests on RC building exterior joints with wide beams. *Adv. Mater. Res.* **2013**, *787*, 771–777. [\[CrossRef\]](#)
- Guo, M.; Huang, H.; Zhang, W.; Xue, C.; Huang, M. Assessment of RC frame capacity subjected to a loss of corner column. *J. Struct. Eng.* **2022**, *148*, 04022122. [\[CrossRef\]](#)
- Lima, C.; Martinelli, E.; Faella, C. Validazione sperimentale di modelli di capacità per nodi interni trave-colonna di strutture in cemento armato. In Proceedings of the Atti del 18 Congresso CTE, Brescia, Italy, 11–13 November 2010; pp. 11–13.
- Astroza, R.; Ebrahimian, H.; Conte, J.P.; Restrepo, J.I.; Hutchinson, T.C. Statistical analysis of the modal properties of a seismically-damaged five-story RC building identified using ambient vibration data. *J. Build. Eng.* **2022**, *52*, 104411. [\[CrossRef\]](#)
- Pappa, R.S.; James, G.H., III; Zimmerman, D.C. Autonomous modal identification of the space shuttle tail rudder. *J. Spacecr. Rocket.* **1998**, *35*, 163–169. [\[CrossRef\]](#)
- Peeters, B.; De Roeck, G. One-year monitoring of the Z24-Bridge: Environmental effects versus damage events. *Earthq. Eng. Struct. Dyn.* **2001**, *30*, 149–171. [\[CrossRef\]](#)
- Magalhães, F.; Cunha, A.; Caetano, E. Online automatic identification of the modal parameters of a long span arch bridge. *Mech. Syst. Signal Process.* **2009**, *23*, 316–329. [\[CrossRef\]](#)
- Reynders, E.; Houbrechts, J.; De Roeck, G. Fully automated (operational) modal analysis. *Mech. Syst. Signal Process.* **2012**, *29*, 228–250. [\[CrossRef\]](#)
- Gentile, C.; Ruccolo, A.; Canali, F. Continuous monitoring of the Milan Cathedral: Dynamic characteristics and vibration-based SHM. *J. Civ. Struct. Health Monit.* **2019**, *9*, 671–688. [\[CrossRef\]](#)
- Alaggio, R.; Aloisio, A.; Antonacci, E.; Cirella, R. Two-years static and dynamic monitoring of the Santa Maria di Collemaggio basilica. *Constr. Build. Mater.* **2021**, *268*, 121069. [\[CrossRef\]](#)

15. Moaveni, B.; He, X.; Conte, J.P.; Restrepo, J.I.; Panagiotou, M. System identification study of a 7-story full-scale building slice tested on the UCSD-NEES shake table. *J. Struct. Eng.* **2011**, *137*, 705–717. [[CrossRef](#)]
16. Fraser, M.; Elgamal, A.; He, X.; Conte, J.P. Sensor network for structural health monitoring of a highway bridge. *J. Comput. Civ. Eng.* **2010**, *24*, 11–24. [[CrossRef](#)]
17. Rainieri, C.; Fabbrocino, G. Automated output-only dynamic identification of civil engineering structures. *Mech. Syst. Signal Process.* **2010**, *24*, 678–695. [[CrossRef](#)]
18. Pan, C.; Ye, X.; Mei, L. Improved automatic operational modal analysis method and application to large-scale bridges. *J. Bridge Eng.* **2021**, *26*, 04021051. [[CrossRef](#)]
19. Moaveni, B.; He, X.; Conte, J.P.; Fraser, M.; Elgamal, A. Uncertainty analysis of Voigt bridge modal parameters due to changing environmental condition. In Proceedings of the International Conference on Modal Analysis (IMAC-XXVII), Orlando, FL, USA, 9–12 February 2009.
20. Nayeri, R.D.; Masri, S.F.; Ghanem, R.G.; Nigbor, R.L. A novel approach for the structural identification and monitoring of a full-scale 17-story building based on ambient vibration measurements. *Smart Mater. Struct.* **2008**, *17*, 025006. [[CrossRef](#)]
21. Ceravolo, R.; Coletta, G.; Miraglia, G.; Palma, F. Statistical correlation between environmental time series and data from long-term monitoring of buildings. *Mech. Syst. Signal Process.* **2021**, *152*, 107460. [[CrossRef](#)]
22. Ubertini, F.; Comanducci, G.; Cavalagli, N.; Pisello, A.L.; Materazzi, A.L.; Cotana, F. Environmental effects on natural frequencies of the San Pietro bell tower in Perugia, Italy, and their removal for structural performance assessment. *Mech. Syst. Signal Process.* **2017**, *82*, 307–322. [[CrossRef](#)]
23. He, L.; Castoro, C.; Aloisio, A.; Zhang, Z.; Marano, G.C.; Gregori, A.; Deng, C.; Briseghella, B. Investigation of a butterfly-arch stress-ribbon pedestrian bridge under ambient excitation: Dynamic identification, FE modelling and parametric optimization. *Procedia Struct. Integr.* **2023**, *44*, 1594–1601. [[CrossRef](#)]
24. Huth, O.; Feltrin, G.; Maeck, J.; Kilic, N.; Motavalli, M. Damage identification using modal data: Experiences on a prestressed concrete bridge. *J. Struct. Eng.* **2005**, *131*, 1898–1910. [[CrossRef](#)]
25. Siringoringo, D.M.; Fujino, Y.; Nagayama, T. Dynamic characteristics of an overpass bridge in a full-scale destructive test. *J. Eng. Mech.* **2013**, *139*, 691–701. [[CrossRef](#)]
26. Dilena, M.; Morassi, A. Dynamic testing of a damaged bridge. *Mech. Syst. Signal Process.* **2011**, *25*, 1485–1507. [[CrossRef](#)]
27. Lauzon, R.G.; DeWolf, J.T. Ambient vibration monitoring of a highway bridge undergoing a destructive test. *J. Bridge Eng.* **2006**, *11*, 602–610. [[CrossRef](#)]
28. Ji, X.; Fenves, G.L.; Kajiwara, K.; Nakashima, M. Seismic damage detection of a full-scale shaking table test structure. *J. Struct. Eng.* **2011**, *137*, 14–21. [[CrossRef](#)]
29. Hien, H.; Mita, A. Damage identification of full scale four-story steel building using multi-input multi-output models. In Proceedings of the Sensors and Smart Structures Technologies for Civil, Mechanical, and Aerospace Systems 2011, San Diego, CA, USA, 6–10 March 2011; Volume 7981, pp. 1206–1212.
30. Gregori, A.; Di Giampaolo, E.; Di Carlofelice, A.; Castoro, C. Presenting a new wireless strain method for structural monitoring: experimental validation. *J. Sens.* **2019**, *2019*, 1–12. [[CrossRef](#)]
31. Di Giampaolo, E.; Di Carlofelice, A.; Gregori, A. An RFID-enabled wireless strain gauge sensor for static and dynamic structural monitoring. *IEEE Sens. J.* **2016**, *17*, 286–294. [[CrossRef](#)]
32. Gregori, A.; Castoro, C.; Di Natale, A.; Mercuri, M.; Di Giampaolo, E. Using commercial UHF-RFID wireless tags to detect structural damage. *Procedia Struct. Integr.* **2023**, *44*, 1586–1593. [[CrossRef](#)]
33. Angiolilli, M.; Gregori, A.; Tonelli, R.; Tonelli, C.; Ciuffetelli, E.; Peditto, A. Structural performance of unreinforced full-scale façade concrete beam-column joint under cyclic load. *Procedia Struct. Integr.* **2023**, *44*, 870–877. [[CrossRef](#)]
34. Nicoletti, V.; Carbonari, S.; Gara, F. Nomograms for the pre-dimensioning of RC beam-column joints according to Eurocode 8. In Proceedings of the Structures, Aalborg, Denmark, 6–8 July 2022; Volume 39, pp. 958–973.
35. Peeters, B.; Roeck, G.D. Reference based stochastic subspace identification in civil engineering. *Inverse Probl. Eng.* **2000**, *8*, 47–74. [[CrossRef](#)]
36. Pasca, D.P.; Aloisio, A.; Rosso, M.M.; Sotiropoulos, S. PyOMA and PyOMA_GUI: A Python module and software for Operational Modal Analysis. *SoftwareX* **2022**, *20*, 101216. [[CrossRef](#)]

Disclaimer/Publisher’s Note: The statements, opinions and data contained in all publications are solely those of the individual author(s) and contributor(s) and not of MDPI and/or the editor(s). MDPI and/or the editor(s) disclaim responsibility for any injury to people or property resulting from any ideas, methods, instructions or products referred to in the content.